Available online at www.sciencedirect.com
SCIENCE DIRECT®
Planetary and Space Science 52 (2004) 789–798
Planetary and Space Science
www.elsevier.com/locate/pss

Optimal orbits for Mars atmosphere remote sensing

Michel Capderou*, François Forget

Laboratoire de Météorologie Dynamique (IPSL), Ecole Polytechnique, F-91128 Palaiseau France

Received 27 June 2003; received in revised form 24 February 2004; accepted 29 March 2004

Abstract

Most of the spacecrafts currently around Mars (or planned to reach Mars in the near future) use Sun-synchronous or near-polar orbits. Such orbits offer a very poor sampling of the diurnal cycle. Yet, sampling the diurnal cycle is of key importance to study Mars meteorology and climate. A comprehensive remote sensing data set should have been obtained by the end of the MRO mission, launched in 2005. For later windows, time-varying phenomena should be given the highest priority for remote sensing investigations. We present possible orbits for such missions which provide a rich spatial and temporal sampling with a relatively short repeat cycle (50 sols). After computation and determination of these orbits, said "optimal orbits", we illustrate our results by tables of sampling and comparison with other orbits.

Keywords: Satellite around Mars; Mars atmosphere; Orbitography; Remote sensing

1. Introduction

The last two spacecrafts successfully put in a low-orbit around Mars, Mars Global Surveyor and Mars Odyssey, are operating in circular Sun-synchronous orbit. The Mars Reconnaissance Orbiter (MRO), to be launched in 2005, is also planned to use a Sun-synchronous orbit. This kind of orbit presents numerous well-known advantages. However, one of these benefits—the satellite overpasses a given location at about the same local time during its entire mission, and thus observes the scene with roughly the same conditions of solar illumination—is fine for surface mapping, but leads to a very poor sampling in terms of local solar time.

Since a comprehensive remote sensing data set of the Martian surface should have been obtained by the end of the MRO mission launched in 2005, it is likely that for later windows, time-varying phenomena and meteorology should be given the highest priority for remote sensing investigations.

Because the diurnal variations of the atmosphere are very large on Mars, Sun-synchronous orbits are not suitable when one wants to study the martian meteorology. For instance, this is problematic when monitoring the diurnal cycle of the hazes and clouds (which is currently poorly observed and yet expected to be an important constraint for Mars climate models; Tamppari et al., 2003), or to study of the dynamics of the thermal tides which are of key importance for the martian atmosphere circulation. The observation of such atmospheric phenomena implies to obtain a local time sampling over a complete sol (martian day), as shown in Fig. 1. At lower altitudes, seasonal variations in the tides reflect the variations in absorption of solar radiation by aerosol, and are most pronounced during dust storm events (Wilson and Richardson, 2000). These episodic storms require relatively rapid scanning of the diurnal cycle to capture the evolution of the tide amplitudes during the growth and decay stages of these poorly known phenomena. Mars Global Surveyor has also revealed the presence of large amplitude longitudinal density variations at high altitude that are of great significance to spacecraft entry operations as well as being of scientific interest. They are now thought to result largely from diurnal-varying thermal tides interacting with the topography (Forbes and Hagan, 2000; Wilson 2002; Angelats i Coll et al., 2004).

To allow the monitoring of the atmosphere at various local time, it is necessary to choose an orbit which is not sun-synchronous. However, choosing the best orbit requires to make a compromise between two constrains:

(1) On the one hand, the coverage of the diurnal cycle must be performed rapidly enough (e.g. a few tens of sols) so that the diurnal evolution of the observed fields can be separated from the annual seasonal evolution (period:

* Corresponding author. Tel.: +33-1-6933-4544.
E-mail address: capderou@lmd.polytechnique.fr (M. Capderou).

0032-0633/$ - see front matter
doi:10.1016/j.pss.2004.03.006

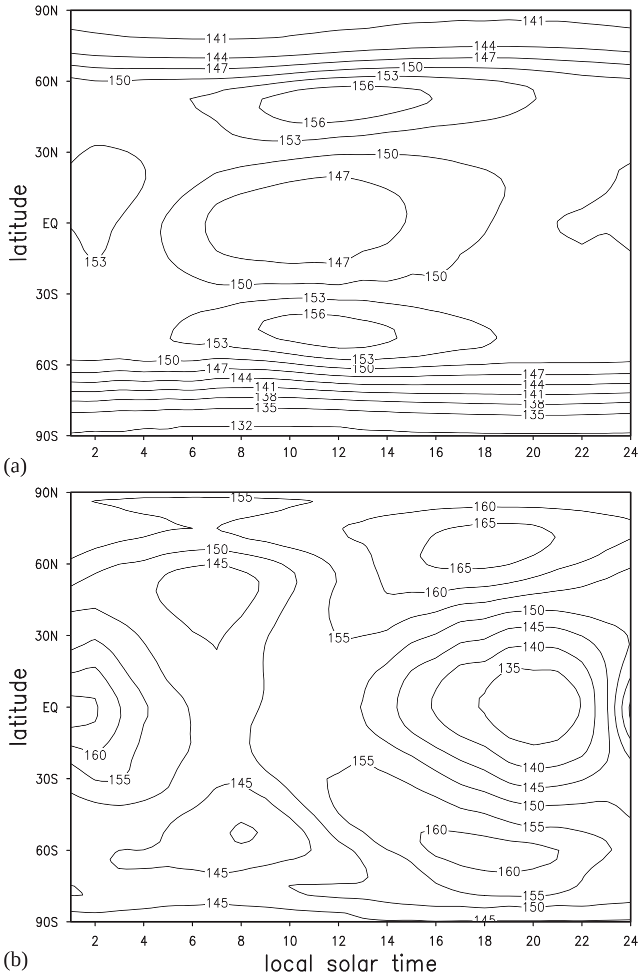

Fig. 1. Examples of atmospheric temperature fields variations in local time (LST) and latitude as predicted by an atmospheric General Circulation Model (Forget et al., 1999) in northern spring (solar longitude $L_s = 0°$–$30°$) (a) at pressure level 7.3 Pa (around 40 km); (b) at 0.12Pa (around 75 km). The large and complex predicted variations are due to thermal tide waves which are of key importance for the martian meteorology and climate (see Zurek et al., 1992; Wilson and Hamilton, 1996). However, very little observations are yet available (see also Wilson and Richardson, 2000). A good sampling of the atmosphere at various local time is necessary to characterize these waves.

669 sols). This implies a relatively low inclination, as shown below.

(2) On the other hand, it is also necessary to observe all latitudes up to the polar regions, since these regions are of key importance to study the water cycle (northern polar cap source), the CO_2 cycle (polar caps), the dust cycle (cap edge dust storms), and the atmospheric dynamic (high latitude baroclinic waves, polar warming, etc.). This requires a high inclination orbit.

In the previous studies, it has often been assumed that sampling the thermal tides with a sufficient latitudinal coverage is impossible (see, e.g. Haberle and Catling, 1996). In this paper, we present the method to obtain the characteristics of an orbit allowing a complete diurnal sampling (over 1 sol), in a short period compared to the seasonal evolution (less than 50 sols), and permitting the observation of the polar regions as well as all longitude. The result is a compromise solution between polar orbit, for pole viewing, and low inclination orbit, for short precession period.

Firstly, we study the viewing geometry and its constraint. Secondly, we compute the nodal precession velocity, giving the precession cycle. We conclude with examples of sampling, illustrating the choice of the orbit. We also examine the effects of resonances that must be taken into account to ensure a good sampling in longitude, and that can be dramatic for orbiters that are also used as relay for surface landers. Although these results are obtained for circular orbits, we add remarks for elliptic orbits.

2. Viewing geometry

The satellite S, altitude h, observes the point P, on the surface of the planet. We consider an across-track swath. Let us note O the center of the planet (considered as spherical, radius R), with N the North Pole, and S_o the subsatellite point. We note the distances: $h = SS_o$, $a = R + h = OS$, and $\eta = a/R$, the relative distance.

The viewing angles (see Fig. 2) are f (half-swath angle), ζ (viewing zenith angle) and α (angle at the center). Nadir viewing (only the subsatellite point S_o is seen by the satellite S) corresponds to $\zeta = 0°$, whereas for an instrument designed to observe the atmospheric limb, the viewing angle is $\zeta = 90°$.

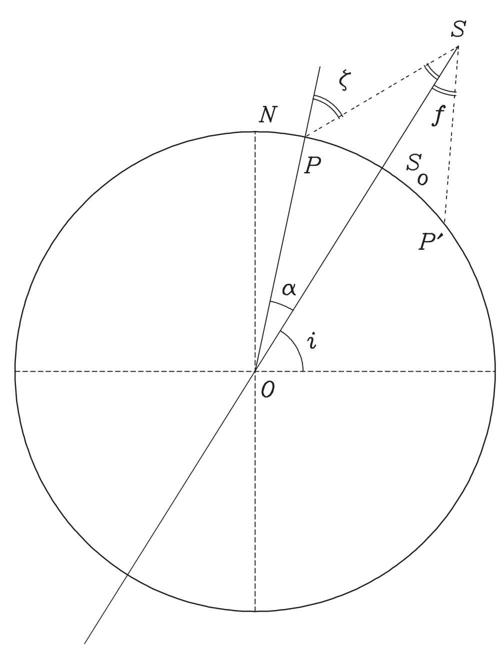

Fig. 2. Viewing geometry, satellite S observing point P by across-track swath.

For a satellite on circular orbit with inclination i, the maximal latitude observed by an instrument (half-swath f) is

$$\varphi = i + \alpha, \tag{1}$$

where φ is the absolute value of the latitude.

By geometric considerations (Capderou, 2003), we obtain the value of α, as function of ζ and η uniquely: $\alpha = \zeta - \arcsin[(1/\eta)\sin\zeta]$. Then, for a defined mission (extreme latitude φ and viewing zenith angle ζ, both fixed), we obtain a relation between the inclination i of the orbit and its latitude h:

$$i = \varphi - \zeta + \arcsin\left(\frac{R}{R+h}\sin\zeta\right). \tag{2}$$

3. Nodal precession velocity

3.1. Precession motion

The intersection of the orbit with the equatorial plane of the planet defines two particular points, the nodes (ascending and descending) of the orbit. The perturbation theory, initialized by Lagrange, shows that the orbital plane (defined by longitude Ω of the ascending node, in a Galilean referential) is submitted to a motion, with pole axis as rotation axis (see for instance, Brouwer and Clemence, 1961; Kaula, 1966). This motion, called *precession motion*, is secular (i.e. proportional to time). It is due to the non-sphericity of the planet and to the action of other celestial bodies. However, the principal cause of this movement is the oblatness of the planet, characterized by the J_2 term of the geopotential. Considering only this term, the velocity $\dot{\Omega}$ of the nodal precession is given by

$$\dot{\Omega}(i,h) = -K_0\left(\frac{R}{R+h}\right)^{7/2}\cos i \tag{3}$$

with K_0 a coefficient which only depends on J_2, on the planet mass M and radius R (Capderou, 2003). For Mars

$$K_0 = 3.074\,84\,10^{-6}\ \mathrm{rad\ s^{-1}} \tag{4}$$

corresponding to $K_0 = 15.640°/\mathrm{sol} = 29.047$ rounds/(martian year).

If the development of the Martian geopotental (Smith et al., 1999; Lemoine et al., 2001) is continued at order n, the expression of $\dot{\Omega}$ is more complex, with terms in $J_2^2, J_4, J_6, \ldots, J_n$ (Capderou, 2003). The relative difference, between the values at order 2 and n, is about 1–2%. In this work, $\dot{\Omega}$ is computed at order 4.

Then, for each orbit, defined by i and h, we obtain, with Eq. (3), the nodal precession velocity, $\dot{\Omega}(i,h)$. The longitude Ω is a measurement of the *Hour Angle*, and $\Omega(t) = \Omega(t_0) + \dot{\Omega}(t - t_0)$ gives directly the *Local Solar Time* (LST) of the ascending node, and consequently the local time of each location overpassed (varying with latitude).

3.2. Precession cycle

The precession cycle is in another way, more vivid, to illustrate the nodal precession velocity. It represents the time interval necessary to obtain the same relative configuration orbit/planet/Sun. The precession cycle C is given by

$$C(h,i) = C = \frac{Y}{\dot{\Omega}_y - 1} \tag{5}$$

with Y the length of the year, and $\dot{\Omega}_y$ the precession velocity expressed in round by martian year (in the case of a Sun-synchronous orbit, $\dot{\Omega}_y = 1$ and C is infinity; in the case of a polar orbit, $\dot{\Omega}_y = 0$, and then and then C is equivalent to one Martian year). Here, C and Y are both expressed in sols (martian days).

For inclinations lower than the Sun-synchronous inclination, the cycle C obtained from Eq. (5) is negative. In this paper, as it is customary, we consider the absolute value of C. The shortest possible cycle is 22 sols: for $i = 0$ and $h = 0$, we have $\dot{\Omega}(0,0) = -K_0$ and $|C| = 669/30.047 = 22.3$ sols.

Important remark: In practice, the ascending and descending nodes are undifferentiated for observation acquiring data, and half a cycle of precession is sufficient to obtain the required sampling.

4. Optimal orbit

In the following study, each case is defined by:

- φ, the highest latitude we wish to reach with an across-track swath,
- ζ, the viewing zenith angle reachable by the instrument (90° for a limb sounder).

Once φ and ζ are set, the orbit precession cycle C only depends on the orbit altitude h, using Eqs. (2) and (5). For instance, Figs. 3a and b illustrate the variation of C as a function of altitude h, for $\varphi = 85°$ and 80°, and various values of ζ.

In these cases, as well in all realistic cases ($\varphi > 70°$, $\zeta > 50°$), one can see that the function $C(h)$ presents a minimum which corresponds to the *best* orbit, according our criteria: For this minimum cycle (shortest period to obtain general sampling), altitude h and inclination i of the orbit are defined, assuring the required conditions of view. It is significant to note that the curve near this minimum is relatively flat (Fig. 3) : for a large variation around the central altitude value of the cycle remains quite the same. This property allows us to define an "altitude interval" for which the half-cycle remains between the optimal minimum value ($C/2$) and ($C/2$) + 1 sol. For this interval, the min-

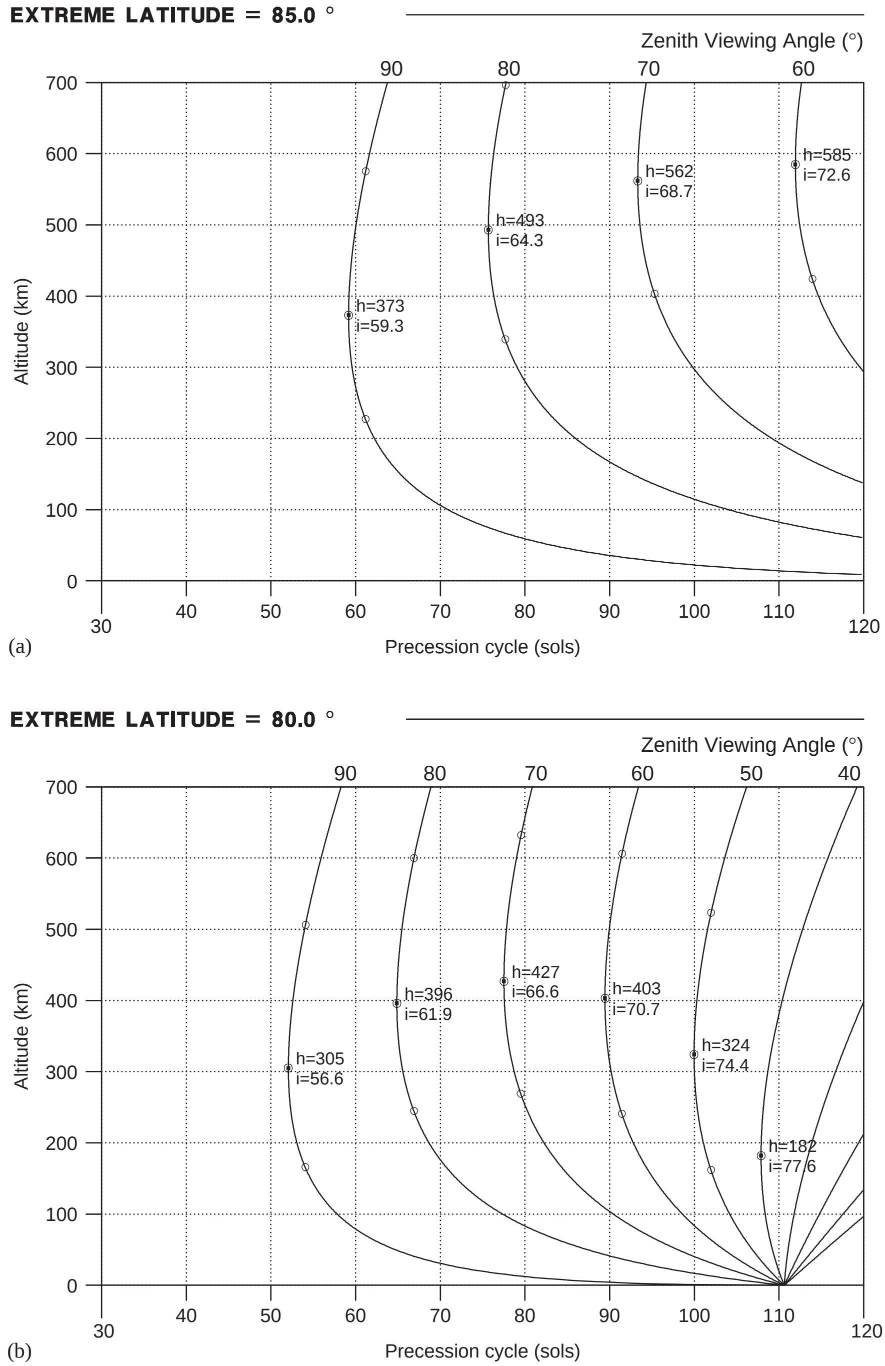

Fig. 3. Precession cycle as function of altitude, for different zenith viewing angles. (a) extreme latitude observed 85°; (b) extreme latitude observed 80°.

imum and maximum altitudes are noted, respectively, h_i and h_s.

In Table 1, we present for each "extreme latitude" φ (from 90° to 50° with a 5° step) and for each maximal viewing zenith angle ζ, the characteristics of the corresponding optimal orbit: half-cycle ($C/2$), inclination i, altitude h and "acceptable" altitude interval $h_i - h_s$. Only the orbits leading to half-cycle less than 90 sols are considered.

5. Viewing angle and sampling for optimal orbit

We present two cases to illustrate the effective advantage of the optimal orbit:

(1) the case of an instrument performing the limb scanning,
(2) the case of an instrument performing around the nadir scanning.

Table 1
Characteristics (h, i) of the optimal orbits for each specifications, giving $(C/2)$

Specif.		Optimal orbit			h limits	
φ (deg)	ζ (deg)	$C/2$ (sols)	i (deg)	h (km)	h_i (km)	h_s (km)
90	50	88	77.6	868	708	1058
90	60	71	74.4	809	648	1003
90	70	57	70.7	726	565	924
90	80	45	66.6	611	453	811
90	90	34	61.9	455	304	656
85	30	86	81.8	371	223	547
85	40	76	79.1	500	345	687
85	50	66	76.0	566	407	760
85	60	56	72.6	585	424	784
85	70	47	68.7	562	403	763
85	80	38	64.3	493	339	696
85	90	30	59.3	373	227	575
80	40	54	77.6	182	24	376
80	50	50	74.3	324	162	523
80	60	45	70.7	403	241	606
80	70	39	66.6	427	269	632
80	80	32	61.9	396	245	600
80	90	26	56.6	305	166	506
75	60	36	68.7	252	90	461
75	70	33	64.3	315	159	523
75	80	28	59.3	315	170	519
75	90	23	53.7	248	117	448
70	70	28	61.9	223	70	432
70	80	25	56.6	249	109	452
70	90	21	50.8	201	79	398
65	80	22	53.7	193	61	395
65	90	19	47.6	163	51	355
60	80	20	50.7	147	24	346
60	90	17	44.4	130	30	318
55	90	16	41.0	103	15	286
50	90	15	37.6	81	6	257

Variation domain (h_i to h_s) allowing half-cycle between $(C/2)$ and $(C/2)+1$. Half-cycles greater than 90 sols are not taken in account. Angles (φ, ζ, i) in degrees, altitudes (h, h_i, h_s) in km, half-cycle $(C/2)$ in sols.

5.1. Limb scanning instrument

Many atmospheric sounders like PMIRR (aboard Mars Observer and Mars Climate Orbiter; McCleese et al., 1992), MCS (aboard the Mars Reconnaissance Orbiter; McCleese, 2003), or MAMBO (initially planned for the CNES Mars Premier Orbiter; Forget et al., 2002) are designed to directly scan the atmosphere at the limb, which corresponds to $\zeta = 90°$. As mentioned above, to reach their scientific objectives, such instruments have to observe the polar regions (e.g. $\varphi > 85°$). According to Table 1, for extreme latitude $\varphi=85°$ and $\zeta = 90°$, the optimal orbit corresponds to an altitude $h=373$ km and an inclination $i=59.3°$, yielding a half-cycle $(C/2)=30$ sols. For altitudes between 227 and 575 km (and adapted inclination), the precession half-cycle is between 30 and 31 sols.

Fig. 4a represents the spatial and temporal sampling for the optimal orbit described above ($h = 373$ km, $i = 59.3°$). For a given meridian, for all the latitudes, we note each overpass (with across-track limb scanning only). We see that, in a 30-sol period, all the latitudes are scanned, between 85°N and 85°S, with homogeneous repartition in space and in local time.

It is very instructive to compare these results with the sampling obtained by a similar instrument (performing across track limb scanning) aboard a Sun-synchronous satellite. We select an MRO-like orbit ($h = 285$ km, $i = 92.7°$, 17-sol repeat cycle, LST of ascending node 15:00), but all Sun-synchonous satellites would give similar results. Fig. 4b represents the spatial and temporal sampling for this MRO-like satellite. In the temporal term, the sampling is very poor, and in spatial term, no latitudes higher than 70° are observed.

5.2. Around nadir scanning instrument

We now choose another kind of swath, with an around nadir scanning instrument. The mission constraints for this instrument are: viewing zenith angle $\zeta = 60°$ and latitude observed up to $\varphi = 80°$. The characteristics of the optimal orbit are noted in Table 1: $h = 403$ km, $i = 70.7$, giving a half-cycle $(C/2) = 45$ sols.

Fig. 5a represents the spatial and temporal sampling for this optimal orbit. For a given meridian, for all the latitudes, we note each overpass (with half-swath $f < 50.7°$ giving a viewing zenith angle $\zeta < 60°$). Within a 45-sol period, all the latitudes are scanned, between 80°N and 80°S, as expected, with homogeneous repartition in space and in local time. The little lacks of sampling, seen in this figure, would be filled if we extend the period up to a complete precession cycle (here, 90 sols).

For comparison, we consider a satellite with the same altitude, but orbiting Mars on a Sun-synchronous inclination. The sampling is obviously very different. As seen in Fig. 5b, most of the planet (between 75°N and 75°S) is observed at only two local time separated by half a sol.

In all fairness, we must note that, due to the eccentricity of the orbit of Mars, the difference between local solar time and local mean time varies between −43 and +53 min (variation known as *equation of time*)—for Sun-synchronous or non-Sun-synchronous missions.

6. Sampling in longitude

Within the "altitude interval" providing a good latitude and local time sampling as described above, the orbit altitude can be further optimized to ensure a good sampling in

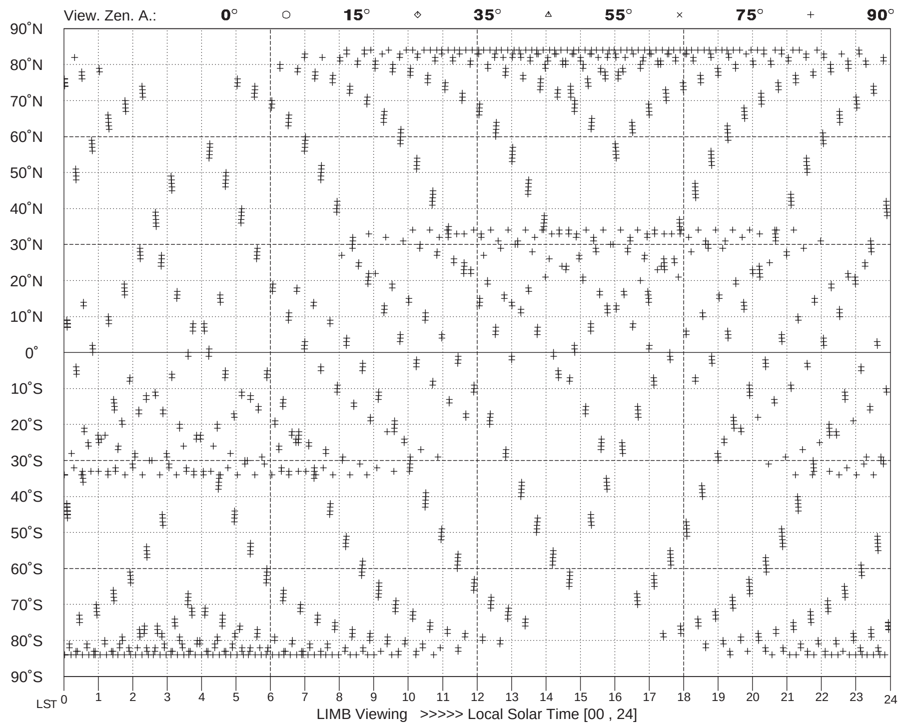

(a)

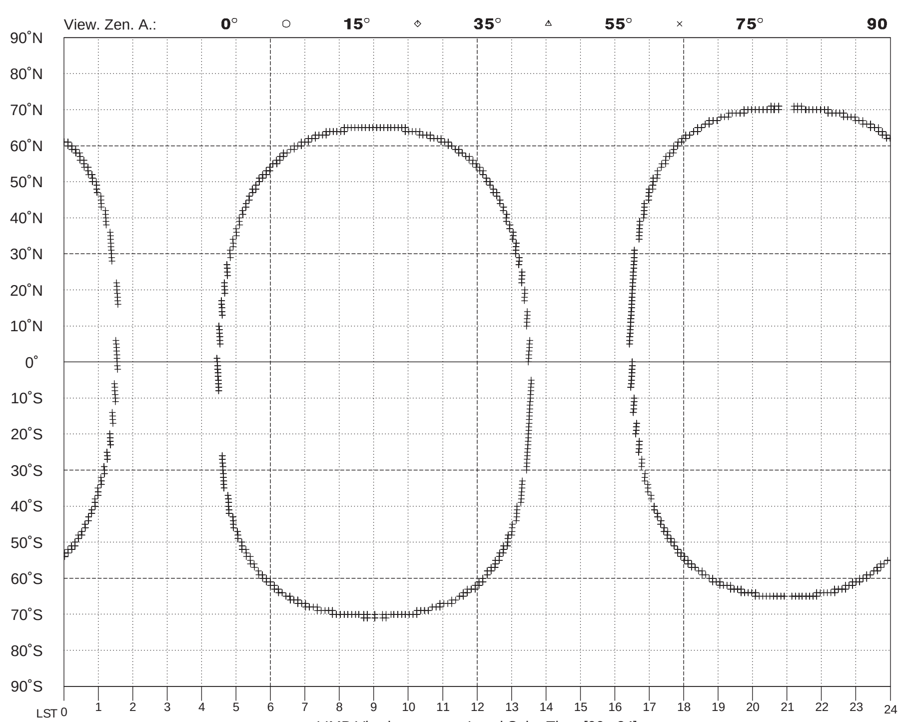

(b)

Fig. 4. Temporal sampling (00:00 to 24:00). Local time sampling (00:00 to 24:00) as function of latitude (from North Pole to South Pole), for an instrument scanning at the limb. Extreme latitude seen: 85°. Time duration: 30 sols (half-cycle of precession). (a) For a satellite on the "Optimal Orbit" described in this paper for these constraints. Orbital data: Altitude $h = 373.0$ km; inclination $i = 59.29°$; period (nodal) $T = 117.09$ min; precession cycle: 59.7 sols. Scanning: $\zeta = 90°$; $f = 64.3°$. First ascending node at 15:00 LST. (b) For a Sun-synchronous satellite, MRO-like (same orbit as for Mars Reconnaissance Orbiter). Orbital data: Altitude $h = 285.1$ km; inclination $i = 92.69°$; period (nodal) $T = 113.30$ min. Scanning: $\zeta = 90°$; $f = 67.3°$. Ascending node at 15:00 LST. Note. For these figures and the following, in the time scale, one hour is corresponding to one martian hour (24 martian hours = 1 sol). Figures by Ixion.

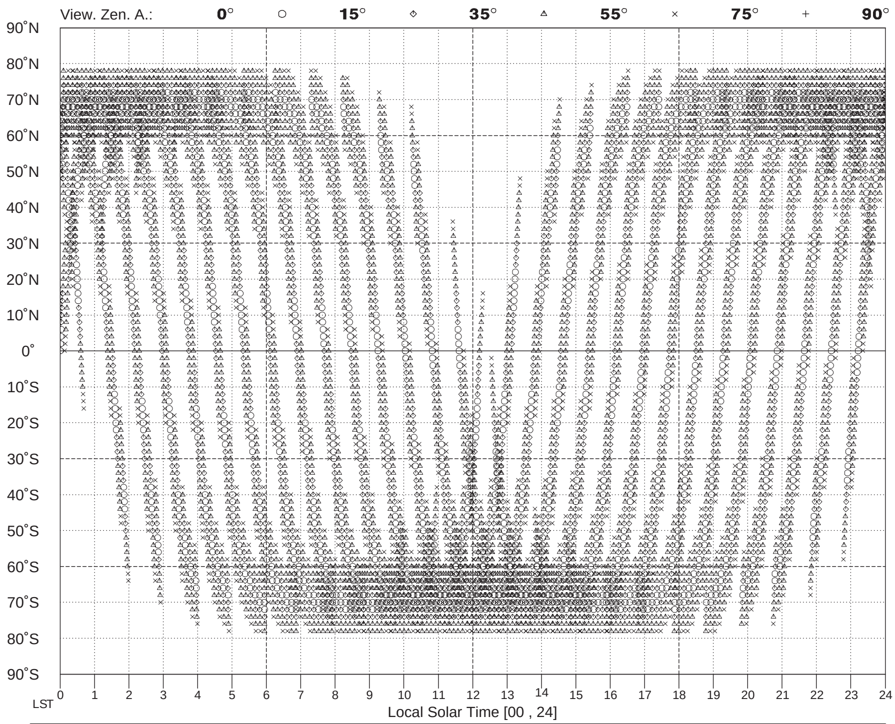

(a)

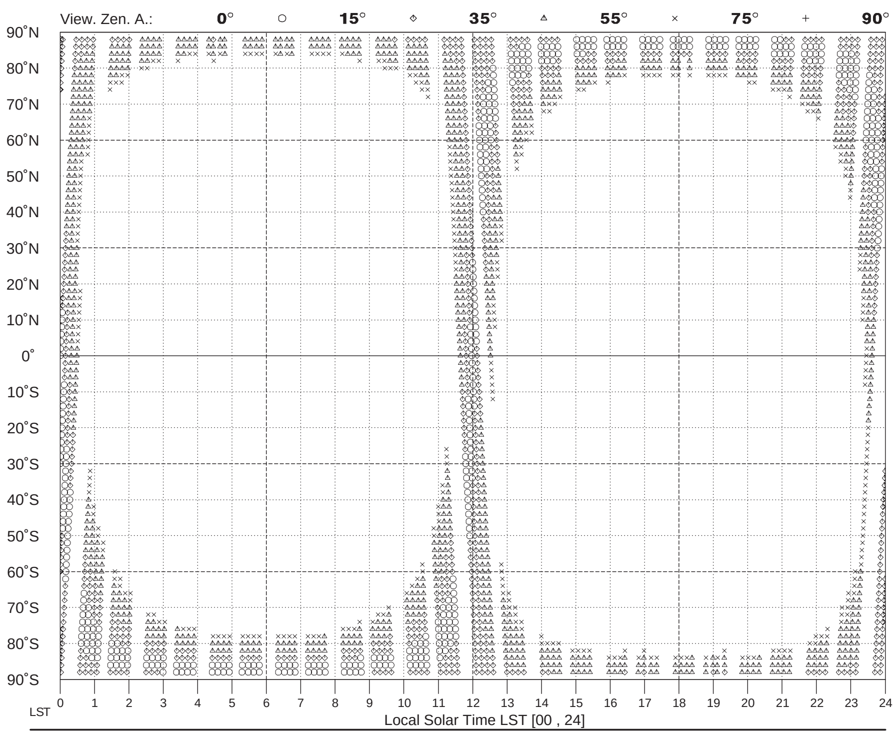

(b)

Fig. 5. Temporal sampling (00:00 to 24:00) as function of latitude (from the North Pole to the South Pole), for two satellites at the same altitude, with the same kind of scanning: $\zeta = 60°$; $f = 50 : 7°$. (a) For a satellite on the "Optimal Orbit" as described in this paper for these constraints. Extreme latitude seen: 80°. Time duration: 45 sols (half-cycle of precession). Orbital data: Altitude $h = 403.0$ km; inclination $i = 70.73°$; period (nodal) $T = 118.65$ min; precession cycle: 90.9 sols. First ascending node at 00:00 LST. (b) For a satellite with the same altitude as a, but with a Sun-synchronous inclination. Time duration: 8 sols (for clear figure - but same configuration for a longer duration). Altitude $h = 403.0$ km; inclination $i = 93.00°$; period (nodal) $T = 118.77$ min. Ascending node at 00:00 LST. Figures by Ixion.

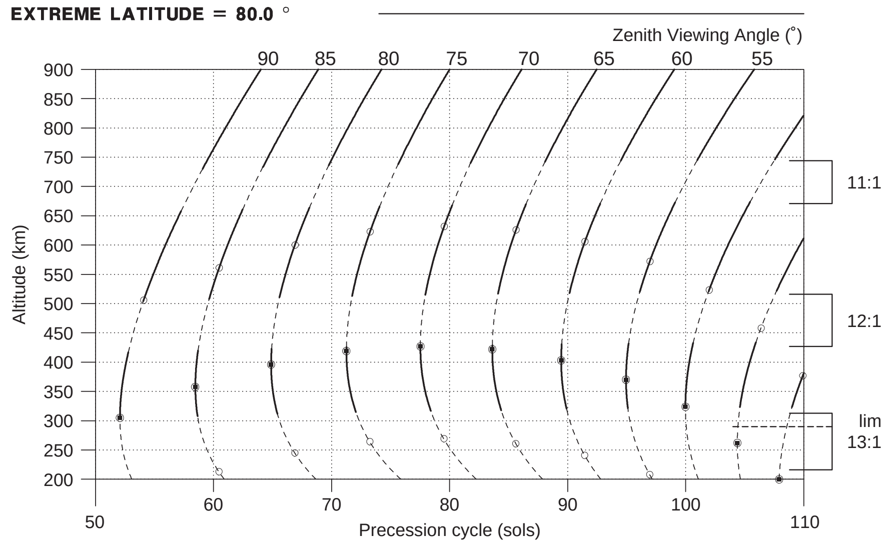

Fig. 6. Precession cycle as function of altitude, for different zenith viewing angles; extreme latitude observed 80°. Same figure as Fig. 3(b), with notation of forbidden zones and their impact for the altitudes, according to resonances. The domain of forbidden zones are centered at resonances (13:1, 12:1 and 11:1), noted in the right margin. Altitudes of forbidden zones are slightly depending on orbit inclination. Below the altitude noted "lim", no complete sampling available in 3 sols.

longitude. A fine and regular sampling in the longitude is indeed required to study the global meteorology or monitor local phenomena (clouds on the flank of a volcanoe, for instance) on a regular basis.

In most cases, high inclination orbits such as the ones described above provide a good longitudinal coverage, thanks to the planet rotation below the orbiter which is much faster than the rotation of the orbital plane. However, depending on the altitude, some orbits tend to overpass some locations on a regular basis and miss the regions in between for long periods (see below). Depending on the science objective of the orbiter, a mission designer can select such a repeatable orbit in order to monitor reference points on a regular basis. However, the extreme cases of this behavior (for instance, if the satellite only fly over 12 longitudes, and nowhere else) should be avoided.

Below, we provide some examples of quantitative analysis conducted in order to further constrain the altitude of our optimal orbits.

6.1. Around nadir scanning instrument

Let us assume that we wish to observe every longitude around the equator (where the longitudinal coverage is the most difficult) with a viewing angle below 45° and in less than 3 sols (days). How constrained is the altitude of the orbit ?

First, let us define the fraction of equatorial coverage $\Phi = L/D$, where L is the length of the Equator seen by the instrument swath, and D, the distance between two consecutive tracks, measured along the Equator. The value of L is close to the swath width (km), but corrected to account for the inclination of the orbit (Capderou, 2003).

We first find that the altitude must be in any case higher than 290 km. For this value, and for $i \sim 65°$, the equatorial shift is $D = 1655$ km and the swath (for viewing zenith angle $\zeta = 45°$) is 514 km, giving for the fraction of equatorial coverage $\Phi = 0.33$.

This value means that the length of the swath is the third of the distance between two consecutive tracks (equatorial shift). Therefore, for altitudes below 290 km, there are *always* gaps in the coverage of equatorial regions in 3 sols. This limit is noted "lim" on Fig. 6.

Above this level, gaps can be created if the orbit tends to fly over the same locations day after day. In practice, that first means that the orbit period must not be close to an exact number of revolutions per sol. Otherwise, the satellite repeats the same coverage day after day and large ground region is never seen by the satellite between two tracks. Within our optimal orbits, 11–13 exact revolutions per sol are possible and must be avoided. Such orbits are described as "resonant" orbits. (resonance 11:1, 12:1 and 13:1, respectively). The exact satellite altitude corresponding to a resonance slightly depends on the orbit inclination (see Table 2). However, the problem is not limited to the exact resonant altitude: orbits with an altitude close to the resonant altitude also provide poor longitudinal sampling. In our example, we can therefore define "forbidden zones" (in altitude) corresponding to the range of altitude that must be avoided in order to allow the observations of every longitude of the equator (and thus on the entire planet) in less than 3 sols and with a viewing angle below 45°.

Using our Ixion numerical model (satellite orbitography and sampling, Capderou, 2003), we determine the altitude limits for each forbidden zone, noted in Table 2.

Table 2
Altitudes, in km, of resonance (z_R) and limits (z_s and z_i, sup. and inf.) of the forbidden zones, as function of the inclination

Forbidden zones		Inclination i (deg)							
Altit.	Resonance	55	60	65	70	75	80	85	S-s
z_s		738	741	744	747	751	755	760	769
z_R	… 11:1	701	703	707	711	715	719	724	733
z_i		665	668	671	675	679	683	688	697
z_s		508	512	516	520	524	529	534	543
z_R	… 12:1	463	467	471	475	479	484	490	499
z_i		420	423	427	431	436	441	447	456
z_s		305	309	313	318	323	329	335	344
z_R	… 13:1	255	259	264	269	274	280	286	296
z_i		207	211	216	221	227	233	239	249

Forbidden altitude zones correspond to the range of satellite altitude that provide an insufficient longitudinal sampling (see text). For satellite in circular orbit. The inclination for Sun-synchronous orbit is noted "*S-s*"

Fig. 6 represents the forbidden zones represented, in Fig. 3(b).

6.2. Limb sounding instruments

An instrument scanning the atmospheric limbs on each side of the orbit only observes two parallel tracks (roughly corresponding to two longitudes in the tropics). The rules described in the previous section also apply here to ensure a good sampling in longitude and thus a complete coverage of the planet. There again, the resonances should be avoided. In the opposite, it can be shown that choosing an orbit altitude exactly in between the resonant orbits can ensure a rapid coverage of all longitude after a few sols (with a few degrees resolution), and a high resolution in longitude after about 50 sols (with about 0.5° resolution)

7. Case of non-circular orbits

The results described above were obtained in the particular case of the circular orbit. Circular orbits are often used in martian missions, but not always. Can we generalize our results to excentric orbit ?

- For elliptic orbits with a low eccentricity $e (e < 0.2)$ the precession motion is about the same as in the case of a circular orbit. The velocity of the nodal precession is given by

$$\dot{\Omega}(i,h) = -K_0 \frac{1}{(1-e^2)^2} \left(\frac{R}{a}\right)^{7/2} \cos i, \tag{6}$$

where a represents the semi-major axis, K_0 being defined by (4). The comparison with Eq. (3), where $R + h = a$, shows a correction of the factor $F = (1-e^2)^{-2} \simeq 1 + e^2$, very close to 1.

For example, for Mars Reconnaissance Orbiter (MRO), $a = 3681.251$ km, $h_a = 312.5$ km (apoapsis), $h_p = 257.6$ km (periapsis), $e = 0.007455$, thus $F = 1.00011$, representing a relative correction of 10^{-4}.

- Orbits with high eccentricity ($e > 0.2$), pose other problems that are out of the scope of this paper. With such orbits, the altitude and the velocity of the spacecraft (and thus the conditions of observations) are significantly different at apoapsis and periapsis. The Mars Express mission provide a recent example of such an orbit. In most cases, an hemisphere (north or south) is favored depending on the latitude of the periapsis, which itself varies with a secular motion (apsidal precession), except for orbit close to the critical inclination ($i = 63°$ or $117°$). Obviously, such orbits are not ideal to monitor the atmosphere with a good spatial and temporal sampling.

8. Case of relay orbiters

A significant part of the future Mars Exploration will also take place on the surface using landers or rovers to perform in situ analysis. Such missions usually use relay orbiters to communicate with the Earth, and the choice of orbit for future spacecrafts should be consistent with a relay function (as it was the case for Mars Observer, Mars Global Surveyor, Mars Oddyssey, Mars Express or Mars Reconnaissance Orbiter).

In theory, non Sun-synchronous orbit like the one proposed in this paper are not ideal for this purpose since they will inevitably go through "dawn-dusk" phases during which the available solar power for surface modules will be low when communication will be possible. However, since we tend to select orbit with high precession cycle, the problem should be only significant for periods a few sols (but several times per year).

Since the duration of the contact between the lander and the orbiter is only a few minutes for low circular orbits, communication should be achievable using batteries.

A more serious issue is that the interval between each contacts should be short enough to command the lander and download the data on a regular basis. Three sols is usually considered the minimum acceptable. Assuming that a suitable contact is ensured if the satellite (as seen by the Lander) is at least 45° above the horizon, it happens that the problem is exactly similar to the one addressed above in Section 6 (our goal there was to observe every point at least every 3 sols and with a viewing angle of less than 45°). Therefore, one can show that the optimal orbit altitude must be chosen outside the forbidden zone corresponding to the resonances, as shown in Fig. 6.

9. Conclusion

For missions requesting complete temporal sampling in local solar time (00 to 24) in a relatively short period (less than 50 sols) and a quasi-complete spatial sampling in latitude and longitude, it is possible to select suitable circular orbits using judicious choices of the orbital parameters.

References

Angelats i Coll, M., Forget, F., Lopez Valverde, M.A., Lewis, S.R., Read, P.L., 2004. The upper atmosphere of Mars up to 120 km: 2. Mars global surveyor accelerometer data analysis with the LMD general circulation model. J. Geophys. Res. Vol. 109, E01011. doi: 10.1029/2003JE002163.2004.

Brouwer, D., Clemence, G.M., 1961. Methods of Celestial Mechanics. Academic Press, New York.

Capderou, M., 2003. Satellites—Orbits and missions. Springer, Berlin, Paris (Chapter 10 : Satellite of Mars) (in French) 504 pp. [English version, Springer, in 2004].

Forbes, J.M., Hagan, M.E., 2000. Diurnal Kelvin wave in the atmosphere of Mars: toward and understanding of “Stationary” density structures observed by the MGS accelerometer. Geophys. Res. Lett. 27, 3563–3566.

Forget, F., Hourdin, F., Fournier, R., Hourdin, C., Talagrand, O., Collins, M., Lewis, S.R., Read, P.L., Huot, J.-P., 1999. Improved general circulation models of the Martian atmosphere from the surface to above 80 km. J. Geophys. Res. 104, 24155–24176.

Forget, F., Beaudin, G., Deschamps, A., Encrenaz, P., Gheudin, M., Thomas, B., Capderou, M., Dassas, K., Ricaud, P., Urban, J., Frerking, M., Gulkis, S., Janssen, M., Riley, L., Encrenaz, T., Lellouch, E., Hartogh, P., Clancy, T., 2002. Microwave sounding of the Martian atmosphere with MAMBO. Geophys. Res. Abstr. 4, 02A04727.

Haberle, R.M., Catling, D.C., 1996. A micro-meteorological mission for global network science on Mars: rationale and measurement requirements. Planet. Space Sci. 44, 1361–1383.

Kaula, W.M., 1966. Theory of Satellite Geodesy. Blaisdell Publ. C., Waltham, MA.

Lemoine, F.G., Smith, D.E., Rowlands, D.D., Zuber, M.T., Neumann, G.A., Chinn, D.S., Pavlis, D.E., 2001. An improved solution of the gravity field of Mars (GMM-2B) from Mars global surveyor. J. Geophys. Res. 106 (E 10), 23359–23376.

McCleese, D.J., 2003. Objectives of the Mars climate sounder (MCS)/Mars reconnaissance orbiter. International workshop (CNES-ESA): Mars atmosphere modelling and observations, Granada.

McCleese, D.J., Haskins, R.D., Schofield, J.T., Zurek, R.W., Leovy, C.B., Paige, D.A., Taylor, F.W., 1992. Atmosphere and climate studies using the mars observer pressure modulator infrared radiometer (PMIRR). J. Geophys. Res. 97, 7735–7757.

Smith, D.E., et al., 1999. The global topography of Mars and implications for surface evolution. Science 284, 1495–1503 (May 28).

Tamppari, L.K., Zurek, R.W., Paige, D.A., 2003. Viking—era diurnal water–ice clouds. J. Geophys. Res. 108, 1–9. CiteID 5073, DOI 10.1029/2002JE001911.

Wilson, R. Evidence for nonmigrating thermal tides in the Mars upper atmosphere from the Mars global surveyor accelerometer experiment. 2002. Geophys. Res. Lett. 29(7), 10.1029/2001GL013975.

Wilson, R.W., Hamilton, K., 1996. Comprehensive model simulation of thermal tides in the Martian atmosphere. J. Atmos. Sci. 53, 1290–1326.

Wilson, R.J., Richardson, M.I., 2000. Infrared measurements of atmospheric temperatures revisited. Icarus 145, 555–579.

Zurek, R.W., Barnes, J.R., Haberle, R.M., Pollack, J.B., Tillman, J.E., Leovy, C.B., 1992. Dynamics of the atmosphere of Mars, In: Mars, pp. 835–933, University of Arizona Press, Tucson.